Supporting Information for

Proton Dissociation and Delocalization Under Stepwise Hydration of Zeolite HZSM-5

John H. Hack[1], Xinyou Ma[1,2], Yaxin Chen[3], James P. Dombrowski[3], Nicholas H. C. Lewis[1], Chenghan Li[1,2], Harold H. Kung[3], Gregory A. Voth[1,2], and Andrei Tokmakoff[1]

[1]Department of Chemistry, James Franck Institute, and Institute for Biophysical Dynamics, The University of Chicago, Chicago, Illinois 60637, United States

[2]Chicago Center for Theoretical Chemistry, The University of Chicago, Chicago, Illinois 60637, United States

[3]Department of Chemical and Biological Engineering, Northwestern University, Evanston, Illinois 60208-3120, United States

Table of Contents

I. Methods

S1a. Hydrated zeolite sample preparation

Samples and equipment

The HZSM-5(17) zeolite samples, also referred to simply as HZSM-5, were a gift from Johnson Matthey (HZSM-5, batch N10-ICZ3-120, nominal Si/Al = 15). HZSM-5(45) samples, used for comparison in Figure S4, were characterized in previous work.[1] Chemicals and reagents, purchased and used without further purification: ammonium nitrate (≥ 99.0%, Sigma-Aldrich), cyclohexane (Fisher Chemical, HPLC grade), methanol (Honeywell Fluka, HYDRANAL-methanol dry), ethanol (Decon 200 proof, anhydrous, USP spec), perfluoro(tetradecahydrophenanthrene), mixture of isomers, (>78% sum of isomers (GC), Alfa Aesar). For sample preparation, 5 μm pore size Nylon Net hydrophilic, nonsterile filters were purchased from Merck Millipore, Ltd. Fluorolube LG-160 (Sigma-Aldrich) and calcium fluoride windows (IR grade optically polished 25 mm dia x 1 mm thick, Crystran Ltd.) were purchased and used as received. An impulse

sealer (Type AIE-205, American International Electric) was used to seal samples in polyethylene bags under a nitrogen atmosphere prior to spectroscopic measurement.

Instrumentation

All air-free manipulations were performed using standard Schlenk techniques on a Schlenk line or in a Vacuum Atmospheres OMNI-LAB glovebox under a nitrogen atmosphere. Thermal equilibration of hydrated samples was performed in a Fisher Scientific Isotemp Programmable Muffle Furnace. Powder X-ray diffraction analyses of zeolite samples were performed at the Integrated Molecular Structure Education and Research Center (IMSERC) at Northwestern University. Elemental analysis of Al, Si, and Na content was performed by the Quantitative Bioelement Imaging Center (QBIC) at Northwestern University using ICP-OES. Measurements were taken using a computer-controlled (QTEGRA software) Thermo iCap7600 ICP-OES instrument (Thermo Fisher Scientific, Waltham, MA, USA) operating in axial view and equipped with a CETAC 520 autosampler (Omaha, NE, USA). Solid zeolite samples (~5-10 mg) were digested by the facility in 3 mL concentrated trace grade nitric acid (> 69%, Thermo Fisher Scientific, Waltham, MA, USA) and 1 mL trace hydrogen peroxide (5% HF, prepared from > 30%, GFS Chemicals, Columbus, OH, USA) and microwaved using the pre-loaded "Silicon Dioxide" OneTouch method (30 min ramp to 180 ^{o}C, 15 min hold, 30 min exhaust). The digested solutions were transferred to pre-weighed 50 mL, metal-free, falcon tubes and triple-rinsed with ultra-pure doubly deionized (DDI) H_2O (18.2 MΩ·cm) to ensure a quantitative transfer. DDI H_2O was then added to produce a final solution of 40 mL total. A quantitative standard was prepared by combining 1000 ug/mL Al, 1000 ug/mL Na, and 1000 ug/mL Si elemental standards (Inorganic Ventures, Christiansburg, VA, USA) to create a 10 ppm Al, Na, Si standard in 7.5% HNO_3 in a total sample volume of 50 mL.

Preparation of dehydrated HZSM-5

The dehydrated HZSM-5 was prepared following a published procedure.[1] Briefly, 5 g of zeolite was calcined at 550 °C (1 °C ramp, 18 h soak, 1 °C cooling to 30 °C, ~200 cc/min O_2 flow), in flowing O_2 for 18 h in a fritted U-shaped quartz reactor. Three ion-exchange cycles were performed on the calcined sample each consisting of a 3 h isothermal treatment at 80°C in 1 M aqueous ammonium nitrate solution under stirring (120 RPM) while sealed within a 500 mL polyethylene bottle inserted into a temperature-controlled silicone oil bath. Samples were filtered through nylon net mesh disc filters (5 μm pore size; 44 mm diameter) in water. Solution with filtered zeolite was centrifuged and dried under vacuum (<100 mtorr) for 24 h. A second calcination was performed at 550 °C, converting the ammonium-form zeolite into the proton-form. Samples were dehydrated by heating to 450 ^{o}C (2 °C min^{-1} ramp to 450 °C, hold for 12 h, 3 °C min^{-1} cooling to 100 °C) under vacuum (~40 millitorr), then sealed without breaking vacuum and transferred to a glovebox for storage. The Si/Al ratio was confirmed by inductively-coupled plasma–optical emission spectroscopy (ICP-OES). Its powder X-ray diffraction (XRD) pattern is shown in Fig. S1. The FTIR spectrum (Fig. S2) confirms the absence of water in dehydrated sample.

Preparation of zeolite containing quantitative amounts of water

The zeolite containing quantitative amounts of water was prepared using a protocol modified from a previously published procedure.[1] In a nitrogen-filled glovebox, dehydrated zeolite (500 mg to 1.500 g) was added to the Teflon insert of a 5 mL Parr Acid Digestion Vessel. Water was added directly to a dehydrated zeolite powder using a micro-syringe, targeting specific numbers of molar equivalents relative to the aluminum content of the zeolite (Al:Si = 1:17). 1 equiv. refers to 1 H_2O molecule per Al atom. Immediately after the addition, the Teflon insert was capped with the Teflon top and hand-sealed in the vessel. The

assembled vessel was removed from the glovebox and tightened using a spanner wrench assembly, and then placed into an oven at 150 °C overnight. After cooling to ambient temperature, the assembly was returned to the glovebox, where the vessel was opened and the Teflon insert removed. After breaking the cap-body seal the powder was quickly transferred to a vial of minimal volume to contain the powder and stored capped and taped in the glovebox until use.

Titration of water in the zeolite

The amount of water loaded onto the zeolite was determined by extraction with methanol following a procedure established for HZSM-5.[2] In a nitrogen-filled glovebox, a known quantity of sample (100~400 mg) was added to 2 mL anhydrous alcohol solvent consisting of 98% methanol and 2% ethanol as internal standard. The resulting slurry was stirred in a sealed vial for 36 h to extract the H_2O into the alcohol solvent. The slurry was filtered (0.2 μm syringe filter) and the water extracted was determined by gas chromatography (Agilent GC Model 6890) calibrated for water relative to ethanol in methanol solvent.

IR sample preparation

In a nitrogen-filled glovebox, ~200 mg of an oil matrix was added to a 20 mL glass scintillation vial and ~100 mg of zeolite sample that was ready for measurement was quickly weighed and transferred to the vial. The oil matrix was comprised of a mixture of Fluorolube LG-160 oil and perfluoro(tetradecahydrophenanthrene) whose ratio was dependant on the hydration extent of the zeolite sample (pure F for > 5 eq. H_2O samples; 2:1 F:P for < 5 eq. H_2O samples). The suspension was mixed thoroughly using a plastic spatula to form a thick mull. Afterwards, the mull was placed between two 1-mm CaF_2 windows and removed from the glovebox for IR spectroscopic measurement.

S1b. IR spectroscopy, decomposition, and modeling

Linear spectroscopy

FTIR spectra were collected with a *Bruker Tensor 27* instrument (800-8000 cm^{-1}, 6 mm aperture, 32 scans, 0.5 cm^{-1} resolution) and baseline corrected. Spectra containing water were scaled to the water stretch-bend combination band near 5260 cm^{-1} and the measured H_2O loading to account for pathlength differences. The spectrum of dehydrated zeolite was normalized to the Fluorolube C-F overtone at 2320 cm^{-1} such that this feature is eliminated upon subtraction of the dehydrated spectrum.

Spectral decomposition

The spectral decomposition into component spectra and hydration dependence was performed by a maximum entropy reweighting of the singular value decomposition (SVD) based on the method of Widjaja and Garland.[3] The final result decomposes the spectral series $A_{kv,}$ with concentration (hydration) index k and frequency index v, into n area-normalized component spectra S_{nv} with hydration dependence C_{kn} and relative frequency-integrated absorption cross-sections ε_n.

$$A_{kv} = \sum_n C_{kn} \varepsilon_n S_{nv} \qquad \text{S(2)}$$

First, the SVD decomposition was performed with n singular values ξ_n.

$$A_{kv} = \sum_n U_{kn} \xi_n V_{nv} \qquad \text{S(3)}$$

Inserting a transition matrix T_{nn} introduces a reweighting of the component spectra $V_{n\upsilon}$ and concentration dependence U_{kn}:

$$A_{k\upsilon} = \sum_n U_{kn} T_{nn}^{-1} T_{nn} \xi_n V_{n\upsilon} \qquad \text{S(4)}$$

where the new component spectra $S_{n\upsilon}'$ and concentration dependence c_{kn}' are

$$\begin{aligned} S'_{n\upsilon} &= \sum_n T_{nn} \xi_n V_{n\upsilon} \\ c'_{kn} &= \sum_n U_{kn} T_{nn}^{-1} \end{aligned} \qquad \text{S(5)}$$

To adjust the reweighting, the transition matrix T is optimized with respect to the objective function F, given by

$$F = H + \gamma^c P^c + \gamma^\upsilon P^\upsilon + \gamma^D D \qquad \text{S(6)}$$

which accounts for information entropy H, positivity constraints P^c and P^υ on the concentration dependence and component spectra respectively, and spectral dissimilarity D. The relative weighting of these constraints is set by the γ^j terms, where j is a superscript. The entropy term penalizes complicated spectral components, given by

$$\begin{aligned} H &= -\sum_n \sum_\upsilon h_{n\upsilon} \ln(h_{n\upsilon}) \\ h_{n\upsilon} &= \frac{S'_{n\upsilon}}{\sum_\upsilon \left| \frac{\partial}{\partial \upsilon} S'_{n\upsilon} \right|} \end{aligned} \qquad \text{S(7)}$$

The spectral positivity term penalizes spectra with negative absorbance, given by eqn. S(8). The concentration positivity is given by replacing $S_{n\upsilon}'$ by c_{kn}'.

$$\begin{aligned} P^\upsilon &= \sum_n \sum_\upsilon f(S'_{n\upsilon})(S'_{n\upsilon})^2 \\ f(x) &= \begin{cases} 0, & x \geq 0 \\ 1, & x \leq 0 \end{cases} \end{aligned} \qquad \text{S(8)}$$

The spectral dissimilarity penalizes similar spectra, calculated by the angle between spectral components when treated as vectors.

$$\begin{aligned} D &= \sum_n \sum_{j>n} D_{nm} \\ D_{nm} &= \begin{cases} 0, & |\theta_{nm}| \geq \pi / 4 \\ 1, & |\theta_{nm}| < \pi / 4 \end{cases} \\ \cos(\theta_{nm}) &= \frac{\sum_\upsilon (\hat{S}_{n\upsilon} \hat{S}_{m\upsilon})}{\sqrt{\sum_\upsilon \hat{S}_{n\upsilon}^2 \sum_\upsilon \hat{S}_{m\upsilon}^2}} \end{aligned} \qquad \text{S(9)}$$

After the maximum-entropy reweighting, component spectra are integrated to obtain the area-normalized spectra S_{nv} and new concentration dependencies c_{kn}. Here, $S_n'(\omega)$ is simply the discrete S_{nv}' treating frequency as a continuous variable ω.

$$\begin{aligned} N_n &= \int d\omega S'_n(\omega) \\ c_{nk} &= c'_{nk} N_n \\ S_{n\upsilon} &= N_n^{-1} S'_{n\upsilon} \end{aligned} \qquad \text{S(10)}$$

This form is sufficient if the transition dipole moment is constant across the component spectra. Then, c_{kn} represent the partition of the system between states with corresponding spectral signatures S_{nv}. Relative values of c_{kn} will report on the relative partitioning, and absolute values carry the same constant factor which includes the pathlength and frequency-integrated, norm-squared transition dipole moment. However, if the transition dipole moment varies across the component spectra, then it is desirable to account for this by further separating $_{ckn}$

$$c_{kn} = c'_{kn}\, \varepsilon_n \qquad \text{S(11)}$$

where C_{kn} carries only information about the concentration dependence of each component and ε_n carries the relative absorption cross-section. An additional constraint is required to perform this separation. We used the constraint

$$\sum_n C_{kn} = \bar{h}_k \qquad \text{S(12)}$$

where $\bar{h}_k$ is the concentration (mean hydration level) at index k. In other words, $C_n\left(\bar{h}\right)$ is defined such that it represents the average number of water molecules in the state with spectral signature $S_n(\omega)$ as a function of hydration level.

Modified BET model

To model the hydration dependence of the populations C_n, we used a modification of the Brunauer-Emmett-Teller (BET) theory. Our model is identical to the development of that theory, but with the modification that the first two adsorption equilibrium constants K_1 and K_2 are distinct, rather than only K_1. The sequential adsorption of water molecules is written as equilibria between sites of microscopic hydration number h at fractional coverage θ_h and water in the gas phase at partial pressure P_{H2O}.

$$\begin{aligned} &\theta_0 + H_2O \; f \quad \theta_1 \;,\; K_1 \\ &\theta_1 + H_2O \; f \quad \theta_2 \;,\; K_2 \\ &\theta_2 + H_2O \; f \quad \theta_3 \;,\; K_3 = K_4 = \ldots = K_L \\ &\ldots \end{aligned} \qquad \text{S(13)}$$

We assume that all subsequent adsorptions have the same heat of adsorption, which is equal to the heat of liquefaction with $K_L = 1/P_0$ where P_0 is the saturation partial pressure. Then, we can write a system of equations with recursive formula for θ_h, in terms of $x = P_{H2O}/P_0$, $b_1 = K_1/K_L$, and $b_2 = K_2/K_L$.

$$\begin{aligned} \theta_1 &= b_1 \theta_0 x \\ \theta_h &= b_1 b_2 \theta_0 x^h,\; h > 1 \end{aligned} \qquad \text{S(14)}$$

The fractional coverages are constrained by the conservation of adsorption sites. In the context of our system, this constraint implies that adsorption sites are independent, and there is exactly one proton per site, which is reasonable since zeolite channels are hydrophobic in the absence of acid sites.[4]

$$1 = \sum_{h=0}^{\infty} \theta_h \qquad \text{S(15)}$$

Equations S(14) and S(15) can be solved together to find a closed-form solution for θ_0, using the solution to the converging harmonic series $\Sigma_h\, x^h = 1/(1\text{-}x)$, $x < 1$. Then, all θ_h can be calculated according to eqn. S(14).

$$\theta_0 = \frac{1-x}{(1-x)(1+b_1 x)+b_1 b_2 x^2} \qquad \text{S(16)}$$

Next, the total number of adsorbed molecules per site $\bar{h}$ and number of adsorbed molecules per site in a cluster of size h, N_h, can be calculated as follows. To find the analytical solution we make use of $\Sigma_h\, h x^h = x/(1\text{-}x)^2$, for $x < 1$.

$$N_h = h\theta_h \qquad \text{S(17)}$$

$$\bar{h} = \sum_{h=0}^{\infty} h\theta_h = \theta_0 \left(b_1 x(1-b_2) + \frac{b_1 b_2 x}{(1-x)^2} \right) \qquad \text{S(18)}$$

Equations S(17) and S(18) give the distribution of water molecules among cluster sizes and total adsorbed water as a function of partial pressure x, which we do not measure in the experiment. Therefore, we can plot any θ_h or N_h against $\bar{h}$ using x as an implicit variable.

More specifically, we construct a model for C_α, C_β, and C_γ by assigning those spectral components to different adsorbed water molecules. We assume that the first water molecule (which interacts with the proton) can contribute either signature α or β, and all subsequent molecules contribute signature γ. Next, we assume that signature α appears only when $h = 1$ and signature β appears for all $h \geq 2$.

$$\begin{aligned} C_\alpha &= \theta_1 \\ C_\beta &= \sum_{h\geq 2} \theta_h \\ C_\gamma &= \sum_{h\geq 2} (h-1)\theta_h \end{aligned} \qquad \text{S(19)}$$

Since $C_\gamma + C_\beta + C_\alpha = \bar{h}$, all molecules are accounted for. These distributions are then a function of two fit parameters b_1 and b_2, which account for stronger binding of the first and second adsorbed water molecules respectively.

Nonlinear IR spectroscopy

2D IR and TA spectra were collected in the pump-probe geometry using a spectrometer that has been described in detail elsewhere.[1,5–7] Briefly, a Ti:sapphire regenerative amplifier (Coherent Legend USX, 800 nm, 5 mJ pulse energy, 1 kHz, 25 fs) was used to drive IR excitation and detection sources. Excitation pulses were generated by sequential down conversion using a commercial OPA (Light Conversion, TOPAS Prime) followed by difference frequency generation in $AgGaS_2$, resulting in 5 μJ, 50 fs pulses centered at 2500 cm^{-1} with bandwidth 350 cm^{-1} full width at half-maximum. Polarization purity was enforced with a

ZnSe polarizer and 6 mm CaF_2, in addition to the 1 mm CaF_2 sample window, was placed in the pump beam for compression. Detection pulses were generated by filamentation in N_2 gas,[8] resulting in <10 nJ, 50 fs pulses spanning 1000-4000 cm^{-1}. The pump was split into a pair of pulses with time delay τ_1 in a Mach-Zehnder interferometer, with the stationary arm chopped at 500 Hz. Excitation and detection pulses met at the sample in the pump-probe geometry with time delay τ_2. The signal was detected in the frequency domain on a 2x64 pixel HgCdTe array detector (Infrared Associates, MCT-9-128, Infrared Systems Development FPAS-0144). Parallel (S_{ZZZ}) and perpendicular (S_{ZZYY}) signal components were separated with a polarizer and collected simultaneously on the two stripes of the array detector. These signal components can be combined to calculate the isotropic component $S_{ISO} = S_{ZZZZ} + 2S_{ZZYY}$.

Additional steps were taken during data collection to remove artifacts from the scatter of the excitation beam. First, a double chopping scheme was employed by chopping the detection beam at 250 Hz. This doubles the duty cycle, but removes scatter terms from interference with the probe. Second, the signal at τ_2 = -5 ps was collected in 2D IR measurements and subtracted to remove scatter from the interference of both pump beams. In TA measurements, the negative time subtraction is performed by averaging over -6 ps to -5 ps to improve the signal-to-noise ratio. In 2D IR experiments, the Fourier transform over τ_1 removes scatter terms which are τ_1 independent but oscillate in τ_2. This is not the case for TA experiments, and thus an additional step must be taken to remove such scatter terms. TA data were collected in steps of 4 fs, below the Nyquist frequency for 4 μm oscillations, and Fourier-filtered along the τ_2 axis using a Hann window in the frequency domain.

S1c. Spectral calculations, rCEC, and charge assignments

DFT potential minimum structures and harmonic spectra

Harmonic spectral calculations were performed on clusters of 1-3 H_2O molecules near the zeolite BAS. This calculation assumes that the protonated water cluster, at all hydration levels, are described by one or several potential minimum structures at the BAS. Compared to the potential energy surface of a protonated water cluster in gas phase, which has limited numbers of potential energy minima, the cluster at interfaces can have numerous local minima. However, the harmonic approximation is a severe limitation for describing the multi-dimensional anharmonic potential energy surface of water. Thus, we only use this approach to introduce 4 vibrational frequency bands for the OH modes.

Since searching for all possible potential energy minimum structures embedded in the zeolite unit cells is computational very expensive with DFT theory, only a few representative configurations are chosen as initial guesses for the searches. An efficient way to screen these initial guess structures is to use a few low-energetic configurations in a long AIMD trajectory. Next, upon obtaining each potential minimum structure, a full-dimensional normal mode analysis is performed at the same theory level of electronic structure calculations. The Hessian matrix is diagonalized to calculate the harmonic frequencies:

$$Hessian = L^{-1}\Lambda L \qquad \text{S(20)}$$

where Λ is a diagonal matrix with the normal mode frequencies λ_i that corresponds to the atomistic motion described by the i^{th} component in the eigenvector L. Thus, we could represent each harmonic vibration mode represented by its largest components of atomic displacements. The harmonic vibrational spectra for 1-3 H_2O cluster at the BAS are shown in Figures S15-S17 for the vibration modes above 1300 cm^{-1}.

Protonic charge rCEC analysis

The position and delocalization of protonic excess charge was quantified for all protonated water cluster configurations in the AIMD trajectories using the rCEC method developed by Li *et* al.[9,10] The rCEC approach, based on the multi-state empirical valance bond (MS-EVB) method developed by the Voth group, firstly assigned the excess proton to different deprotonated molecules/moieties to establish several diabatic states based on different covalent and hydrogen bonding topologies. For example, in a gas phase protonated water dimer, the two diabatic states are H_2O_{w1}---$[H\text{-}O_{w2}H_2]^+$ and $[H_2O_{w1}\text{-}H]^+$---$O_{w2}H_2$; and in a 1 H_2O molecular cluster at the BAS, the two diabatic states at the interfaces are O_z-H---$O_{w1}H_2$ and O_z^----$[H\text{-}O_{w1}H_2]^+$. At higher hydration levels, since the water cluster could donate hydrogen bonds at the interfaces, the four oxygen atoms at the BAS were included as possible protonation states. For example, the minimum number of diabatic states is 3 for a 2 H_2O cluster at the BAS, and the diabatic states are: O_z-H---$O_{w1}H_2$---$O_{w2}H_2$, O_z^----$[H\text{-}O_{w1}H_2]^+$---$O_{w2}H_2$, and O_z^---- H_2O_{w1}---$[H\text{-}O_{w2}H_2]^+$. The fourth diabatic state is non-negligible when a hydrogen bond is formed between O_{w2} and O_z' another oxygen at BAS, which leads to an additional protonation state O_z^---- H_2O_{w1}---H_2O_{w2}---H-O_z'. For a total of *n* protonation states, the overall wave function is then representated by an *n* x *n* matrix **H**, following the formalism in the MS-EVB theory. The ground state (adiabatic) wavefunction is then expanded in the basis of *n* diabatic states:

$$\left|\psi^{adiabatic}\right\rangle = \sum_i c_i \left|\psi_i^{diabatic}\right\rangle \qquad \text{S(21)}$$

where c_i is the expansion coefficient for the i^{th} diabatic state. Unlike the original MS-EVB method, where the probability density c_i^2 of a diabatic state wavefunction is calculated by diagonalizing the *n* x *n* matrix **H**, Li and Voth showed that in the rCEC approach c_i^2 can be obtained directly from constrained DFT (CDFT) calculations of the diabatic states.[10] Furthermore, the ratio of the CDFT probability densities for two neighboring diabatic states, namely c_i^2/c_j^2, decreases almost monotonically as the differential hydrogen bond distance $\delta(O_i\text{-}H\text{-}O_j) = r(O_i\text{-}H) - r(O_j\text{-}H)$ decreases. Li and Voth showed[10] that this can be fit by an exponential decay function within the cut-off range $r_{1,ij}$:

$$\frac{c_i^{\,2}}{c_j^{\,2}} = \exp\left[-k_{ij}\left(\delta_{O_i-H-O_j} - \delta_{0,ij}\right)\right] \qquad \text{S(22)}$$

where $k_{ij} = 4.9840$ and $\delta_{0,ij} = 0$ fit the best for proton transfer in liquid water, and $k_{ij} = 7.3433$ and $\delta_{0,ij} = 0.29316$ for proton transfer from amino acid (-COOH) to water. Beyond $r_{1,ij}$, c_i^2/c_j^2 decreases to 0 at $r = r_{2,ij}$ via a polynomial damping function. Therefore, the protonic center-of-excess charge position is a weighted average of the center-of-charge (COC) position for each diabatic state:

$$\mathbf{r}^{CEC} = \sum_i c_i^{\,2}\mathbf{r}_i^{COC} \qquad \text{S(23)}$$

Next, we quantify the delocalization of CEC using the weights c_i^2, where the value of a c_i^2 is ~1 if a protonation state dominates, and $c_i^2 = c_i^2 \sim 0.5$ if two protonation states are equally important. Here, we use the participation ratio (PR) to calculate the delocalization of the protonic excess charge for the molecular complex including the 4 zeolitic O and *h* water molecules:

$$PR = \left(\sum_{i=1}^{h+4} c_i^{\,4}\right)^{-1} \qquad \text{S(24)}$$

To perform rCEC analysis for the protonated water cluster at the BAS, we define the "heavy atom" (water O and zeolitic O) identity (O_ID), the molecule identity (Mol_ID), the point charge on H (Q_H) and O (Q_O), and the number of covalent bonds each heavy atom can form with H in the protonated ($N_{H,protonated}$), and the

total number of H in the deprotonated species (H_total). Specifically, all zeolitic O are assigned to the first molecule (Mol_ID = 0), and the water O are assigned to an individual molecule ID. An example of the rCEC topology definition for a 3 H_2O cluster at the BAS is listed in Table S1.

Table S1. Topology definition parameters used in the rCEC analysis for a 3 H_2O cluster at the BAS.

O_ID	$N_{H,protonated}$	Mol_ID	Q_H	Q_O	H_total
0	1	0	0.50	0.50	0
1	1	0	0.50	0.50	0
2	1	0	0.50	0.50	0
3	1	0	0.50	0.50	0
4	3	1	0.26829	0.19512	2
5	3	2	0.26829	0.19512	2

In addition, since the CDFT parameters are not parameterized specifically for the zeolitic O at the BAS, we tested the k_{ij} and $\delta_{0,ij}$ parameters for proton transfer from water and from amino acid to water, respectively, and the results are almost identical at all hydration levels. Furthermore, tuning the partial charges Q_H and Q_O for the zeolitic O also does not change the CEC distributions nor the PR distributions.

Anharmonic power spectrum analysis of AIMD trajectories

Anharmonic spectra of each water cluster at the BAS are calculated using the velocity-velocity correlation function $C_t(v_0,v_t)=\langle v(0)v(t)\rangle/\langle v^2(0)\rangle$ from the AIMD spectrum followed by a Fourier transform. This is essentially the power spectrum, and we can repetitively calculate this for all atoms in a protonated water cluster. We used the formalism applying the Wiener-Khinchin theorem for power calculations:[11]

$$P(\omega)=\left|\int C_t\cdot e^{-i\omega t}dt\right|^2 \qquad \text{S(25)}$$

where the spectral density is averaged over 10000 replica. Similarly, we used the formalism below to calculate the spectral density for the CEC trajectory[9] $r_{CEC}(t)$:

$$P^{CEC}(\omega)=\left|\int\frac{\left\langle r^{CEC}(0)\cdot r^{CEC}(t)\right\rangle}{\left\langle r^{CEC}(0)\cdot r^{CEC}(0)\right\rangle}e^{-i\omega t}dt\right|^2 \qquad \text{S(26)}$$

which is averaged over 500 replicas. We then use the CEC spectrum as a reference to screen the power spectrum of each atom to exam whether it contains the "proton feature" shown in the CEC spectrum. One of the advantages of using the rCEC approach to trace the protonic charge in the AIMD trajectory is that the bending mode in the flanking water molecules (~1400 cm^{-1}) can be correctly described.[9]

DFT Löwdin charge population distributions

Löwdin charge populations[12] were evaluated using the DFT/revPBE theory for the protonic water cluster configurations every 10 steps (every 5 ps) in the AIMD trajectories. The DFT Löwdin charge of each atom in the protonated water cluster, as well as the 3 zeolitic O closest to them, are shown in Fig. S25 for 1-6 H_2O cluster. Based on the atomic identities, we then assigned the Löwdin charges to their configurational positions Table S2. Compared to the atoms that are geometrically away from the protonic charge, the O and H atoms in the vicinity of the delocalized protonic charge have Löwdin charges shifted to the positive and negative directions, respectively.

II. Supplemental Data

S2a. Sample characterization

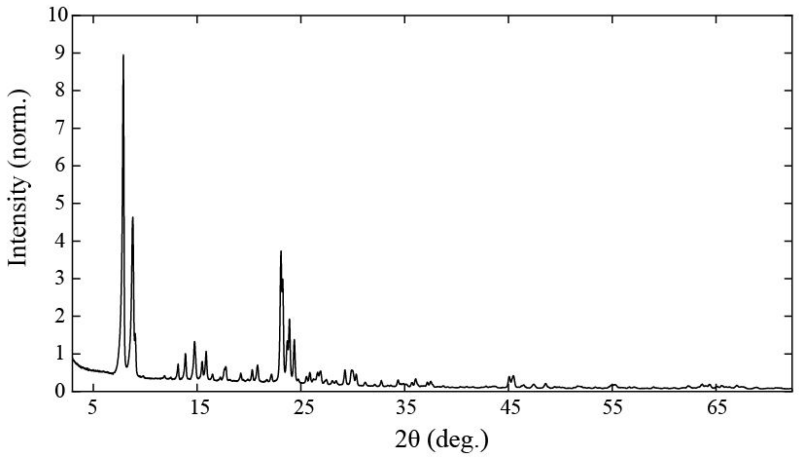

Figure S1. Powder XRD pattern of dehydrated HZSM-5(17).

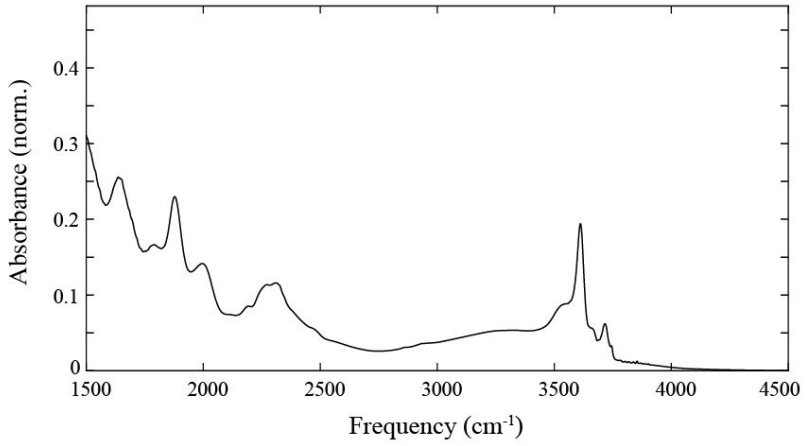

Figure S2. FTIR spectrum of dehydrated HZSM-5(17).

The powder XRD pattern and FTIR spectrum of dehydrated HZSM-5(17) are displayed in Figures S1 and S2, confirming the absence of H_2O under sample preparation conditions.

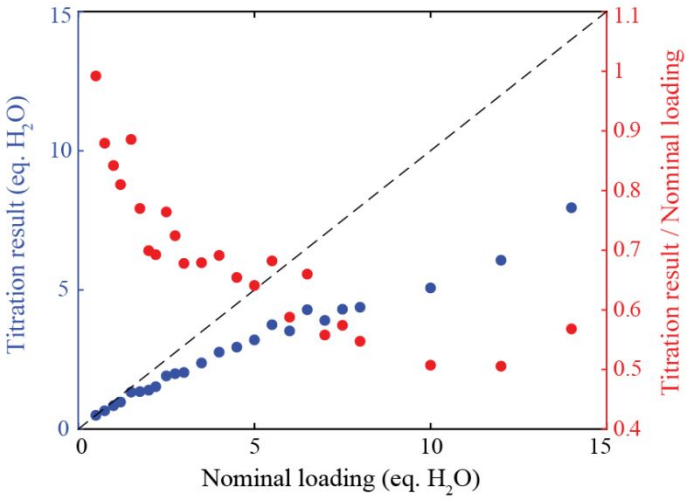

Figure S3. Titration results for different nominal hydration levels of zeolite. The data is displayed in terms of both measured equivalents of H_2O (titration result) and the ratio of measured equivalents to nominal loading. The dashed line denotes equal titration result and nominal loading.

Figure S3 shows the results of titration with methanol to measure the water content of hydrated samples. For samples with lower than 1.5 eq. H_2O/Al site added and equilibrated at 150 °C, 88±7% of the water added initially was measured in the final sample when titrated using the protocol described herein, verifying the efficacy of our titration method. When nominal water loading increases to 8 eq., the ratio of titrated water amount to the nominal water loading decreases to ~50%. After that, the ratio remains constant. The titration result (eq. H_2O measured per Al atom) is used throughout the text.

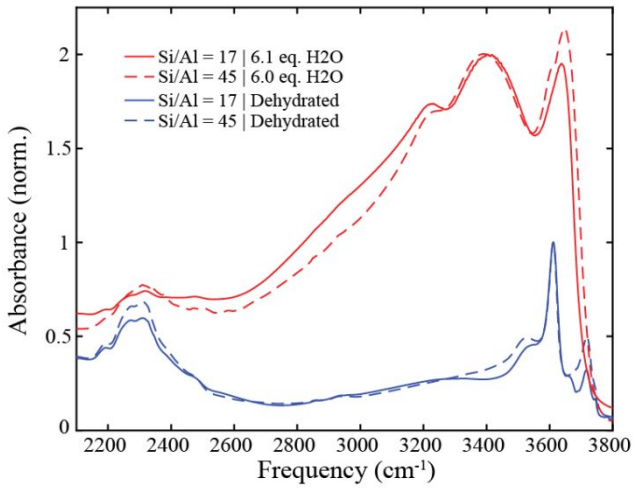

Figure S4. Comparison of FTIR spectra with Si/Al = 17 & Si/Al = 45. Spectra are plotted with both dehydrated zeolite and 6 eq. H_2O. Dehydrated spectra are normalized to the bridging O-H stretch at 3610 cm^{-1}; hydrated spectra are normalized to the H-bonded O-H stretch at 3400 cm^{-1}. Spectral differences with varying Si/Al are minor. Spectra display the same features at the same center frequencies, with small variations in relative intensity.

Figure S4 shows that spectral differences are minor between HZSM-5(17) used here and a HZSM-5(45) sample, which was prepared with similar methodology and described in previous work.[1]

S2b. Linear IR spectroscopy and modeling

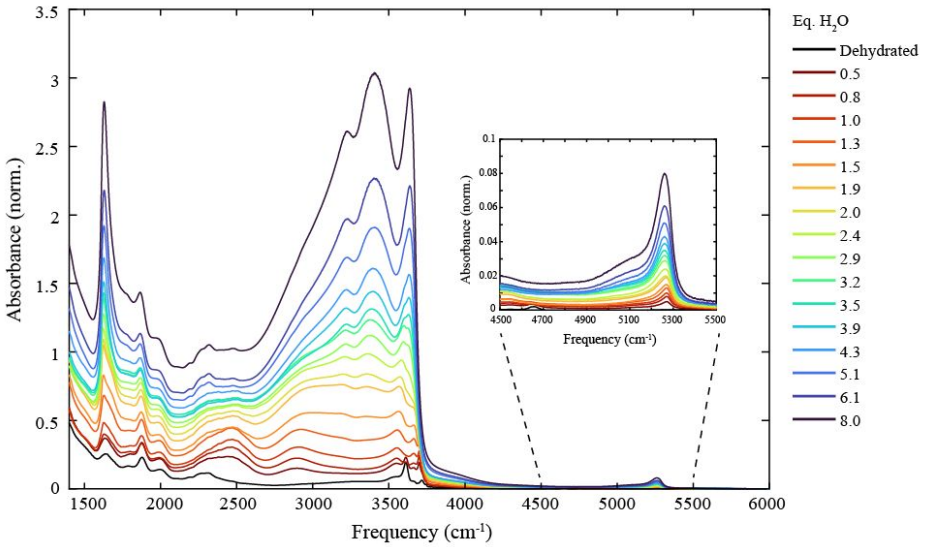

Figure S5. FTIR hydration series of HZSM-5(17) without dehydrated zeolite subtraction. The inset shows a closeup of the water stretch-bend combination band centered at 5260 cm^{-1}.

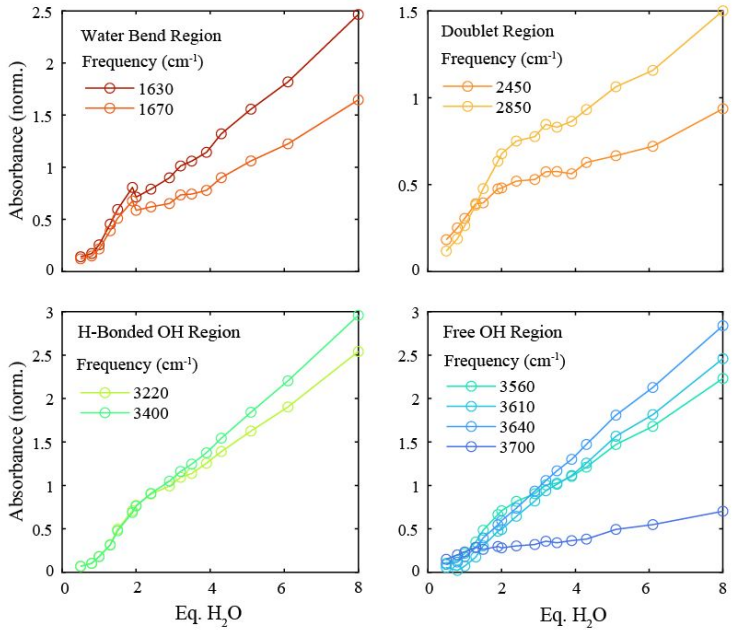

Figure S6. FTIR absorbance trends at selected frequencies.

Figure S5 shows the FTIR hydration series without dehydrated zeolite subtraction. Spectra are scaled to the measured hydration level using the water combination band at 5260 cm^{-1}. Very similar results were obtained by scaling to the integrated area from 1700-4000 cm^{-1}. Absorbance amplitude traces at selected frequencies are plotted in Fig. S6. Frequencies below ~3600 cm^{-1} all display a kink near 2 eq. H_2O, which is absent in trends above that frequency. The behavior is explained by the spectrum and hydration dependence of component 2 in the spectral decomposition (Figure 2).

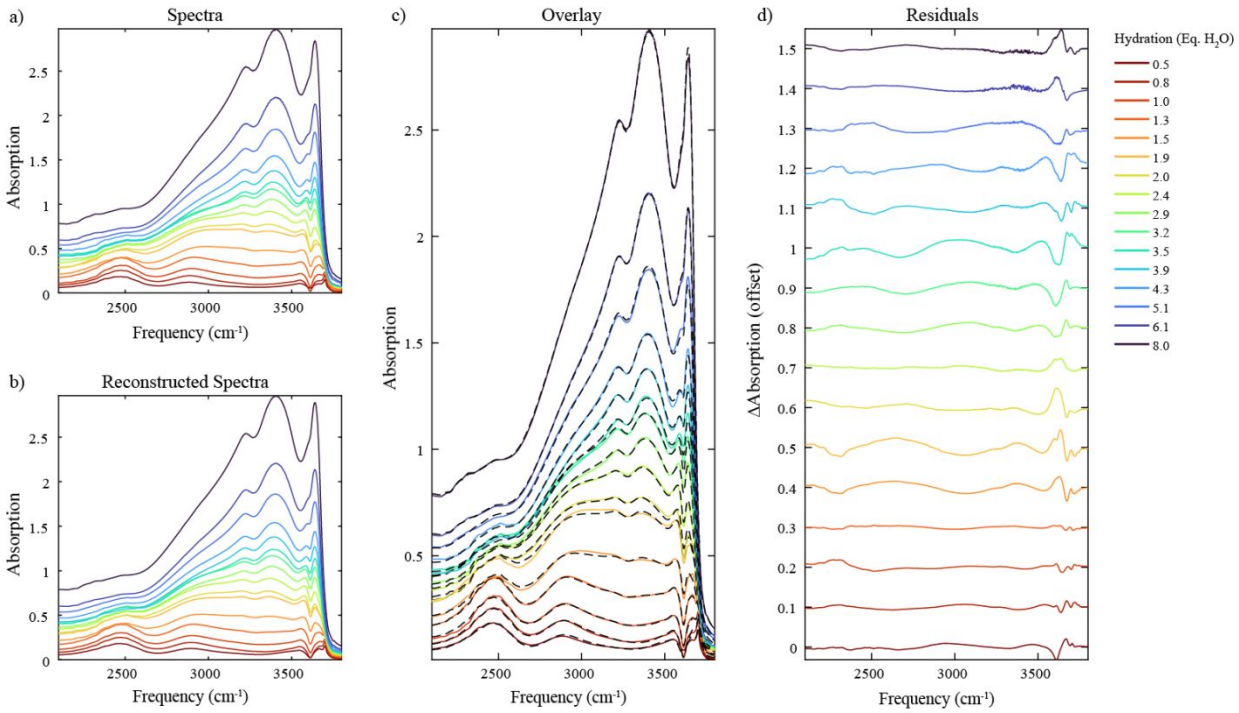

Figure S7. Residuals of spectral reconstruction presented in Figure 2. (a) Measured spectra with dehydrated subtraction. (b) Reconstructed spectra from three spectral components. (c) Overlay of selected spectra with reconstruction. (d) Residuals (reconstructed – measured spectra) at all hydration levels; residuals are offset by 0.1 absorbance units for clarity.

Figure S7 displays the FTIR hydration series reported in Fig. 1, the reconstructed spectra from the decomposition reported in Fig. 2, and the differences between them. This is a measure of the error in that spectral decomposition for describing changes in the IR spectra as a function of hydration. The residuals (reconstructed – measured spectra) in the region below 3500 cm^{-1} are on the order of ~1% of the signal. The largest residuals appear in the free-OH region of the spectrum, but are still small relative to the signal. Using the sum of squared residuals to calculate the coefficient of determination shows $R^2 > 0.999$.

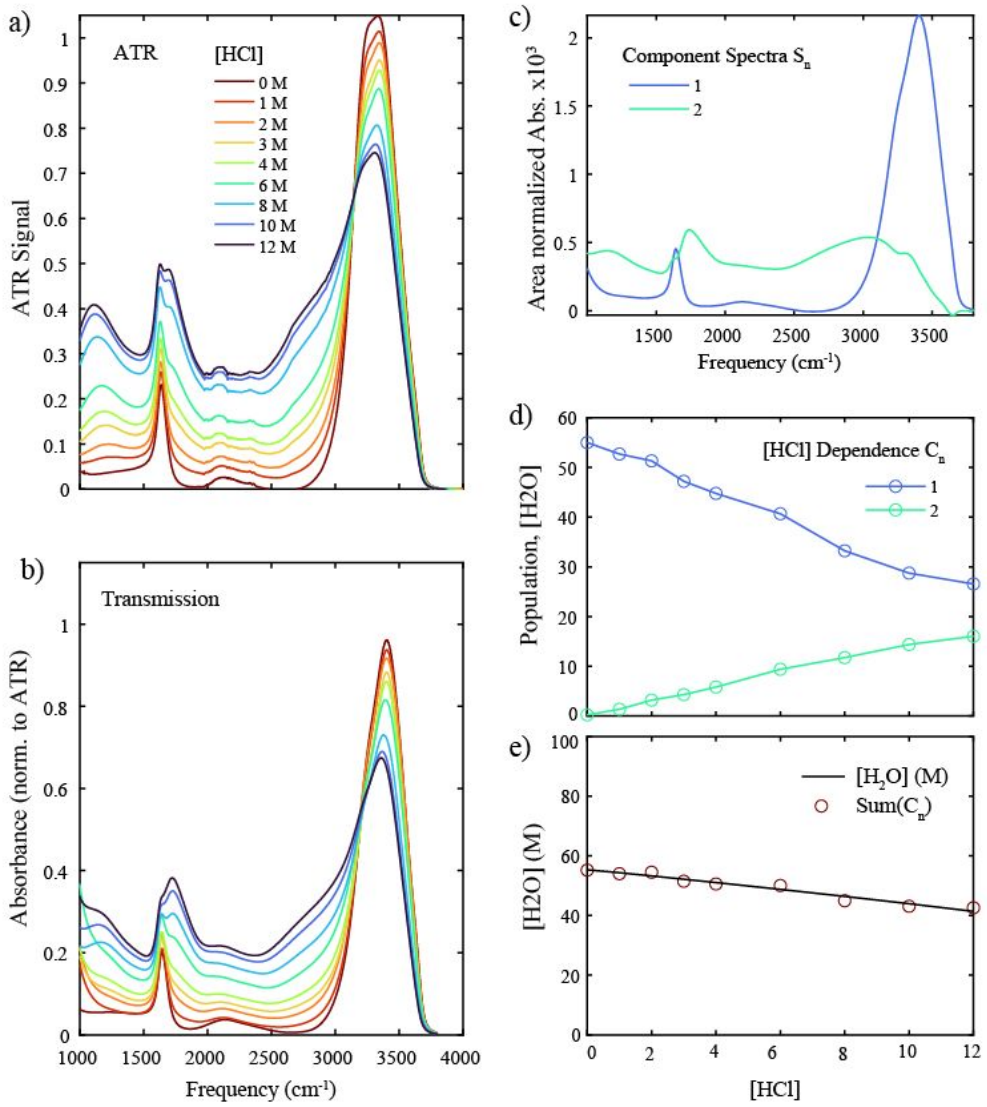

Figure S8. Spectral decomposition of aqueous HCl series. (a) ATR and (b) transmission mode IR spectra of aqueous HCl solution from 0-12M. Transmission mode spectra were normalized to the water stretch at 3400 cm^{-1}. Component spectra (c) and [HCl] dependence (d) for the normalized transmission mode concentration series were calculated using the spectral decomposition method applied in Figure 2. (e) The [HCl] dependence was separated from relative square transition dipole moment factors by constraining the sum of C_n to $[H_2O]$, which was calculated by accounting for the solution density as a function of [HCl]. The calculated extinction coefficient ratio was $\varepsilon_2/\varepsilon_1 = 4.8$.

For comparison to the zeolite hydration spectral series, the same decomposition analysis presented in Fig. 2 was applied to a concentration series of aqueous HCl solution, displayed in Fig. S8. The data are described by two components which strongly resemble the IR spectra of H_2O and aqueous proton,[13] and decrease / increase linearly with [HCl] as expected. This suggests that linear spectral decomposition can be reasonably applied to describe the FTIR spectroscopy of a proton in water.

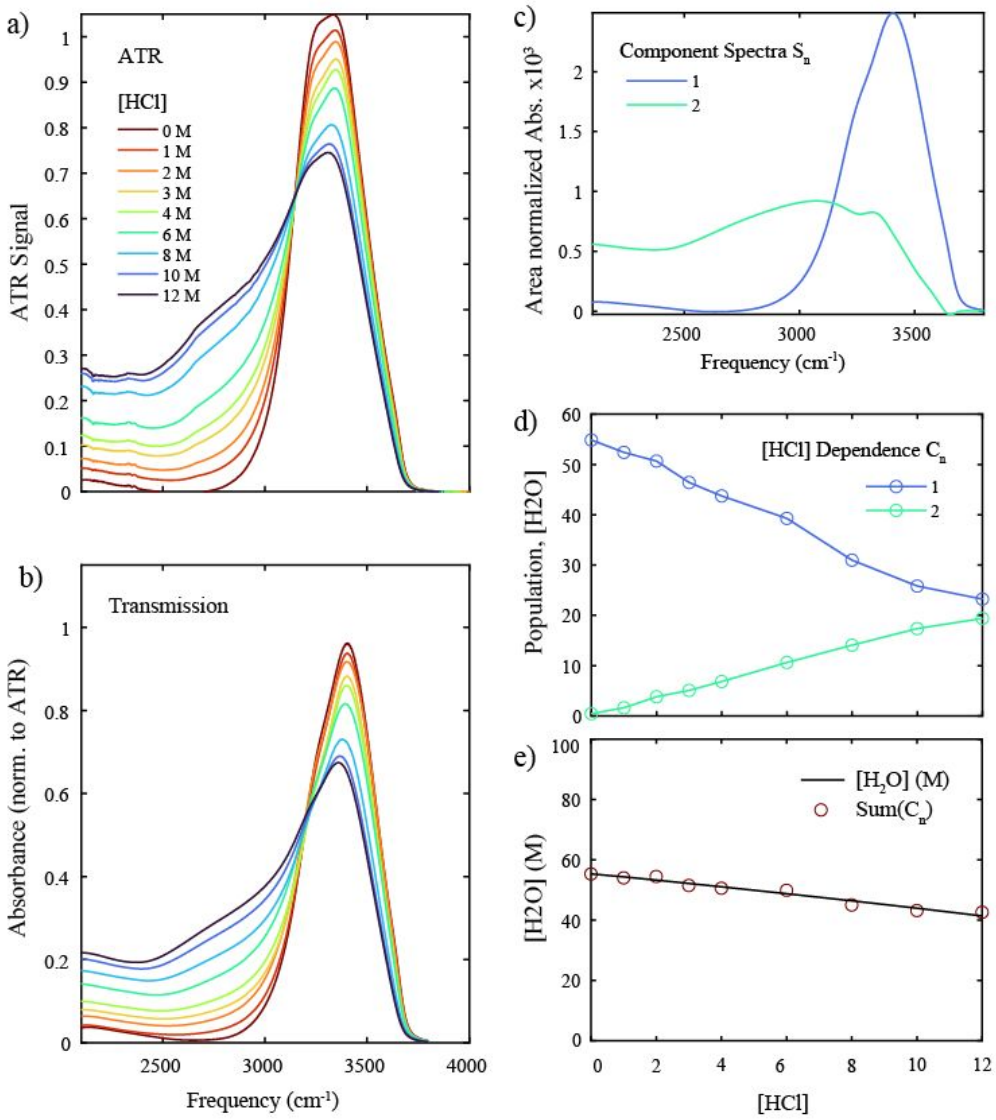

Figure S9. Spectral decomposition of aqueous HCl series with restricted spectral range. The same analysis was performed as described for Figure S8, but the spectral range was restricted to 2100-3800 cm^{-1} – the same range that was used to analyze the HZSM-5 hydration series (Figure 1). (a) ATR spectra and (b) transmission IR spectra of aqueous [HCl] series. (c) component spectra and (d) [HCl] dependence from spectral reconstruction with $\varepsilon_2/\varepsilon_1 = 2.7$ from constraining C_n to $[H_2O]$ as a function of [HCl].

Figure S9 displays the same analysis as Fig. S8, but with the spectral range restricted to 2100-3800 cm^{-1}. The component spectra and hydration dependences are nearly identical to the result when considering a wider spectral range (Fig. S8). The only major difference is the extinction coefficient ratio, which is larger when the spectral range is expanded. This is as expected, since the inclusion of additional transitions will modify the mean square transition dipole moment, integrated across the frequency axis. Therefore, the hydration – or [HCl] – dependencies extracted using this method are robust, but the ratio of extinction coefficients depends on the frequency range considered.

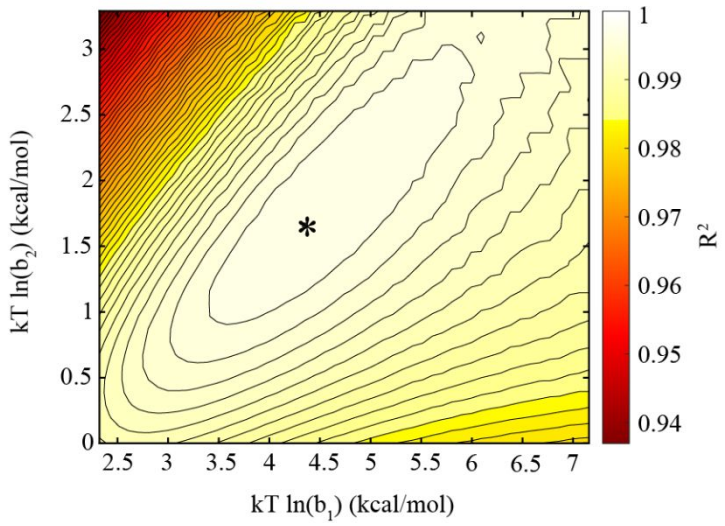

Figure S10. The coefficient of determination R^2 as a function of fit parameters b_1 and b_2 for the two-parameter BET model. The asterisk marks the point of best fit. Labels use T = 423 K which is the preparation temperature.

Figure S10 displays the optimized R^2 value for fitting the two-parameter BET model to the hydration dependence data in Fig. 2. The asterisk marks the point of best fit, corresponding to $b_1 = 180$ and $b_2 = 7$ and the result plotted in Fig. 2. Notably, fit is relatively sensitive to b_2, which shifts the fitted C_β up/down with increasing/decreasing value. The fit is less sensitive to b_1, which could be increased with a relatively small impact on R^2.

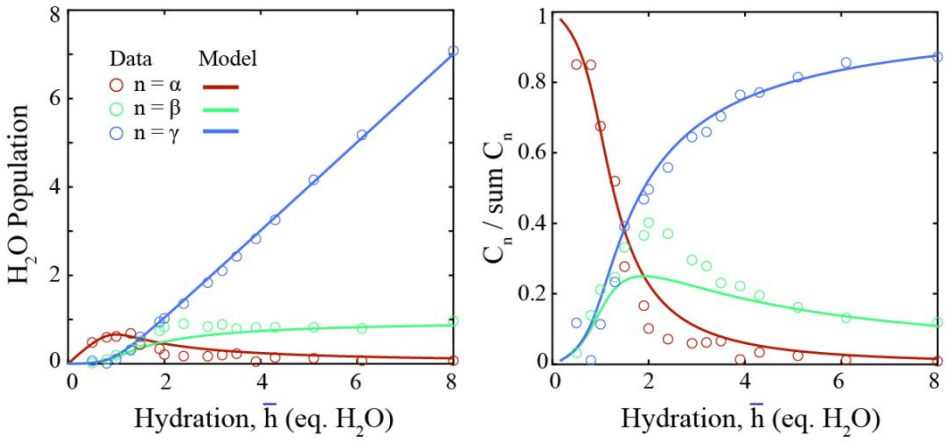

Figure S11. BET model with a single fit parameter $b_1 = 20$ ($b_2 = 1$) plotted against the data reported in Fig. 2 in the main text.

Setting $b_2 = 1$ returns the typical BET model, where only the first adsorption is stronger than the others. Under these conditions, the model fits best with $b_1 = 20$, shown in Figure S4. We see that the data is captured well at low and high values of $\bar{h}$, but that the model underestimates C_β and overestimates C_α near $\bar{h} = 2$. Increasing or decreasing b_1 does not remedy this error and causes disagreement with the data in other regions of $\bar{h}$, so both parameters are necessary to capture the data.

S2c. Nonlinear IR spectroscopy

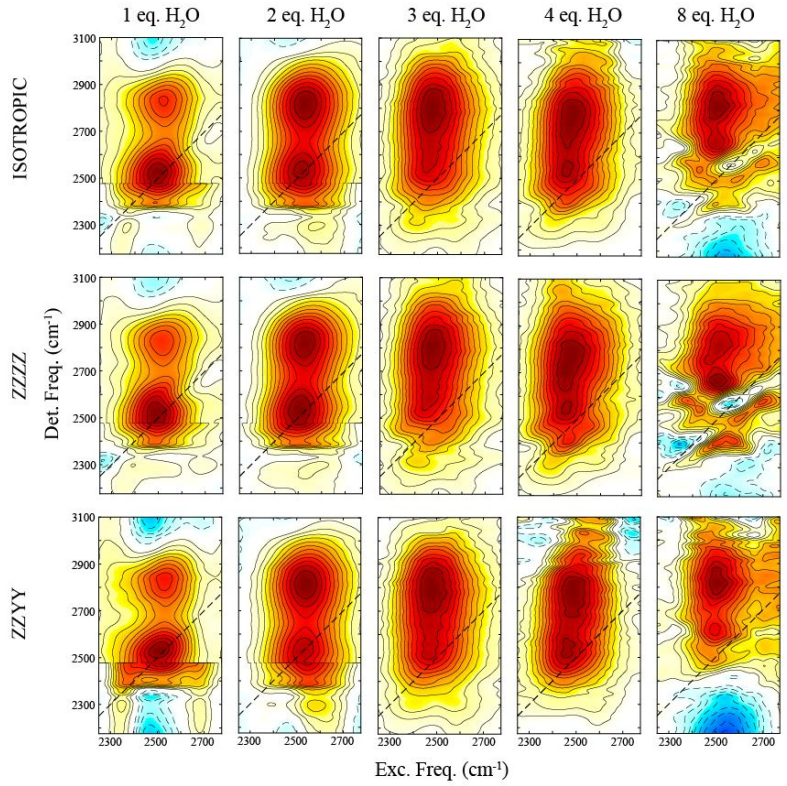

Figure S12. 2D IR spectra of hydrated HZSM-5 at 100 fs waiting time as a function of hydration level and polarization. Parallel polarization between pump and probe is denoted ZZZZ, perpendicular is denoted ZZYY, and isotropic is the combination $S_{ISO} = (S_{ZZZZ} + 2S_{ZZYY})/3$.

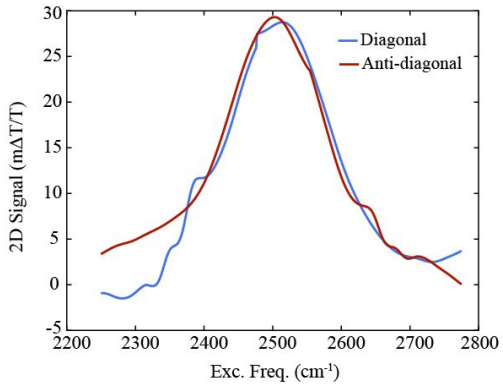

Figure S13. Diagonal and anti-diagonal slices of the isotropic 2D IR spectrum of 1 eq. H_2O at 100 fs. Both have linewidth 170 cm^{-1} FWHM.

Figure S12 displays 2D IR spectra as a function of hydration and polarization. Perpendicular (ZZYY) spectra are free of scatter artifacts, while some residual scatter can be observed in the ZZZZ and isotropic spectra of 4 and 8 eq. H_2O. The features are homogeneously broadened, as shown by the equal diagonal and antidiagonal linewidths of 1 eq. H_2O (isotropic) in Fig. S13.

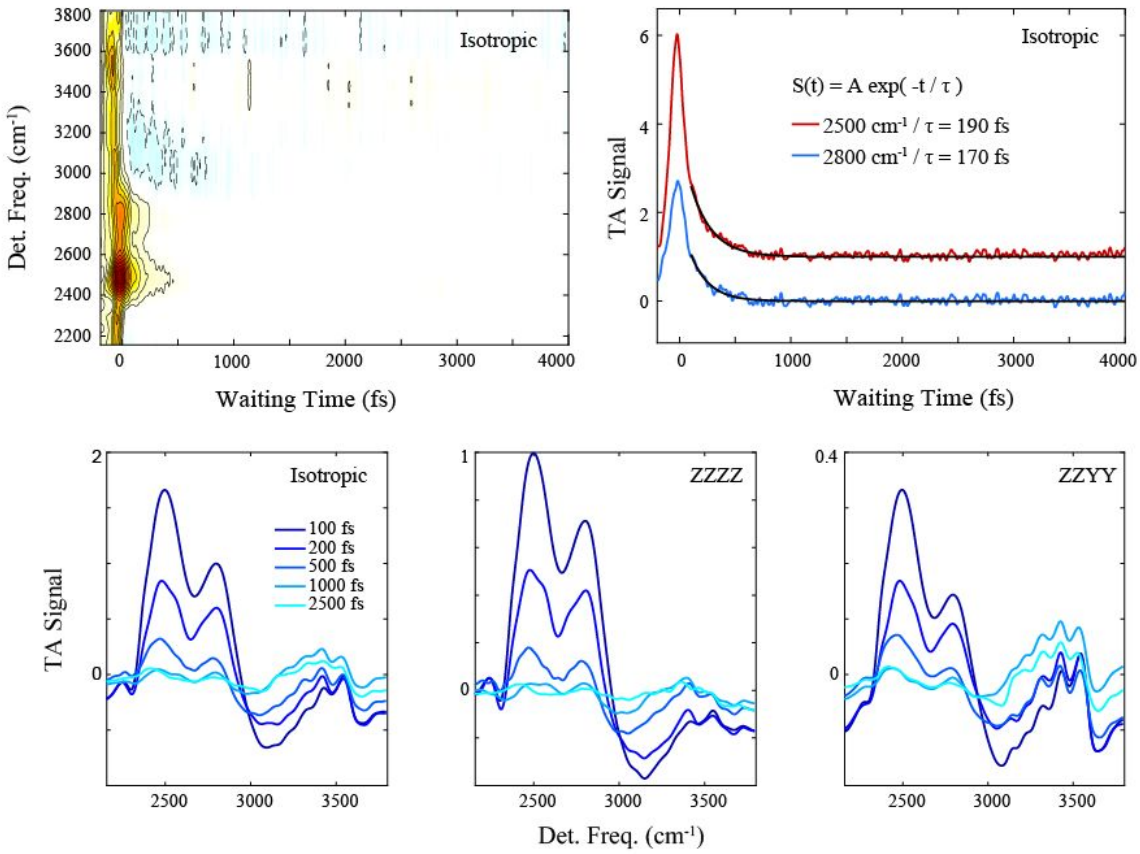

Figure S14. Transient absorption spectrum of 1 eq. H_2O / HZSM-5 after excitation centered at 2500 cm^{-1}. Isotropic time traces at selected detection frequencies were fit to a single exponential to extract population relaxation timescales. Time traces were fit to $\tau_2 \geq 100$ fs to exclude the nonresonant response from pulse overlap. Black lines represent the fits, and traces were offset for clarity. Isotropic, parallel (ZZZZ), and perpendicular (ZZYY) frequency slices are displayed as a function of waiting time.

The transient absorption spectrum of 1 eq. H_2O is displayed in Fig. S14. The isotropic spectrum at a detection frequencies of 2500 cm^{-1} and 2800 cm^{-1} were fit to single exponentials with population relaxation timescales of 190 fs and 170 fs, respectively.

S2d. Harmonic spectral calculations

Harmonic normal modes were calculated for optimized structures of 1,2, and 3 H_2O clusters adsorbed at the BAS. Figures S15-S17 display the structures considered and their corresponding harmonic spectra.

1 H_2O cluster

At the lowest hydration level, the optimized structure shown in Figure S15 has interfacial OH distances of 1.05 and 1.54 Å for the O_z—H and the H—O_w bonds, respectively. Thus, the interfacial hydrogen leans towards the zeolite. The 5 OH vibration modes in Figure S15 are assigned to four types based on visualizing their motions: 1) O_z—H bend at ~1400 cm^{-1}, 2) water H-O_w-H bend at ~1600 cm^{-1}, 3) the interfacial stretch O_z—H---O_w, at ~2200 cm^{-1}, and 4) free OH stretch at >3500 cm^{-1}. The potential minimum structure of 1 H_2O molecular cluster is similar to the representative configuration in the AIMD simulation (shown in Figure 4).

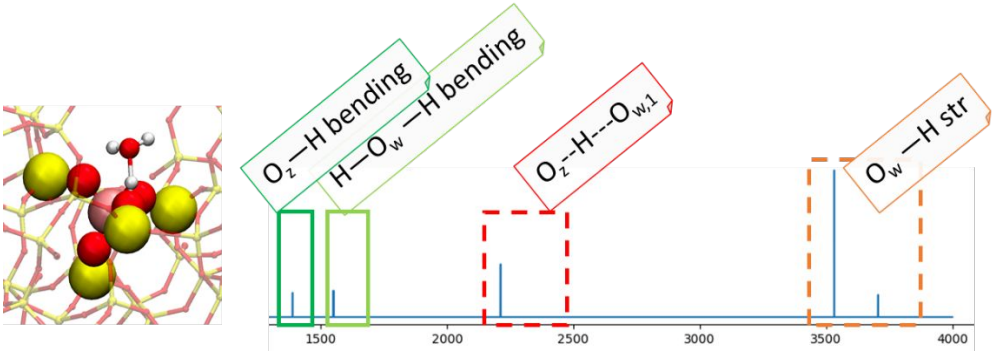

Figure S15. The potential minimum structure and harmonic frequency stick spectrum (wavenumber unit: cm^{-1}) assigned to four types: O_z-H (green), H-O_w-H bend (light green), O_z-H---O_w stretch (red), and O_w-H stretch (orange).

2 H_2O cluster

As the number of hydrogen bonds increases in the 2 H_2O cluster, the protonated cluster at the BAS can have multiple potential energy minimum configurations. To avoid searching for similar configurations, we randomly sampled 10 configurations from the AIMD trajectory of 2 H_2O cluster at 300 K, which are used as the initial guess to search for potential energy minimum structures. Among the 10 potential minimum structures, three types of configurations are unique (shown in Figure S15): a) O_z-H---(H_2O_{w1})---(H_2O_{w2}), i.e., the interfacial H is closer to O_z, b) a $[H_2O_{w1}$--H--$O_{w2}H_2]^+$ cluster that donates two hydrogen bond from both water moieties, and c) O_z---$HO_{w1}H_2$---($O_{w2}H_2$), i.e., similar to a) but the interfacial H is closer to O_{w1}. Compared to the 1 H_2O cluster harmonic spectrum, the vibrational mode at 1300~1500 cm^{-1}, becomes a H_3O^+ umbrella mode in b) and c). The interfacial mode is ~2400 cm^{-1} in configuration a) as a O_z-H stretch, and this becomes the interfacial O_z---H-O_w stretch in configuration b) and c) which span in the range of 1900~2800 cm^{-1}.

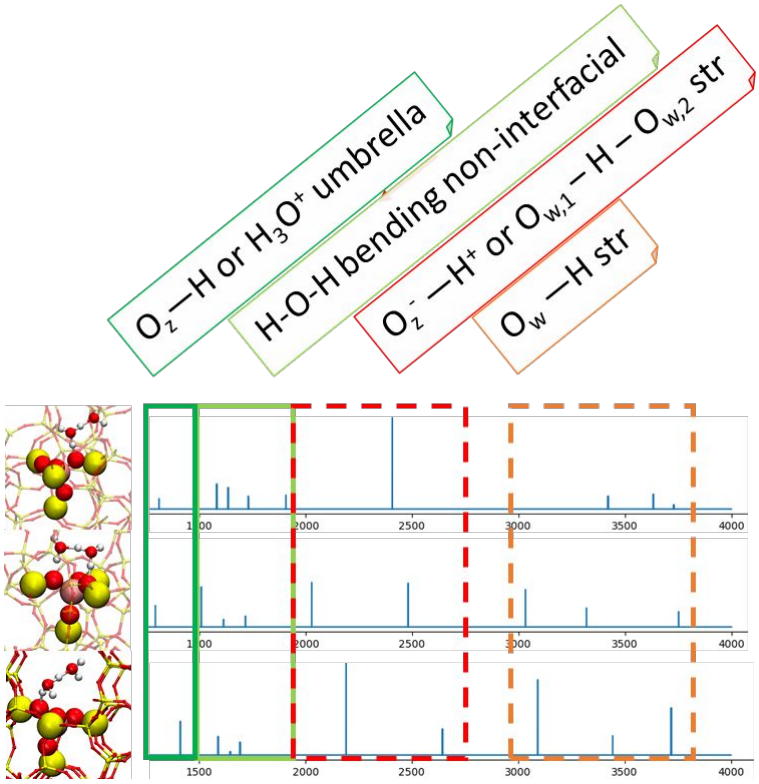

Figure S16. Same as S15 but for 2 H_2O cluster at the BAS. The ~1400 cm^{-1} mode (green) can be either a O_z-H bend or a H_3O^+ umbrella mode, and the proton stretch mode (red) can either be at the interface or flanked by two water molecules.

3 H_2O cluster

The above approach for finding potential energy minima and harmonic spectra for 2 H_2O clusters was also adopted for calculating the harmonic spectrum 3 H_2O cluster in ZSM-5. Here, only 4 unique types of potential minimum structures are located: 1) each of the two terminal water molecules donates a hydrogen bond to the zeolite oxygen, and the central water molecules is slightly out of the interface; 2) a terminal and a central water molecule donate two hydrogen bonds to their nearest zeolitic oxygen atom, respectively, and another water molecule accepts a water hydrogen bond and does not form hydrogen with the BAS oxygen atoms; 3) similar to 2) but the interfacial hydrogen bond is weaker; and 4) all three water molecules donates a hydrogen bond to the zeolitic oxygen atoms. The above vibrational assignments still apply here, except that the ~1400 cm^{-1} mode is now entirely a H_3O^+ umbrella mode. Within the four types, we only see one where the interfacial hydrogen bond is strong enough to show interfacial OH modes at ~2500 cm^{-1}.

Overall, the harmonic approximation is mostly helpful to identify the vibrational modes and establish the correlation between the configuration and the spectrum. However, since the O-H modes are often highly anharmonic the harmonic spectral calculation will not capture anharmonic shifts or couplings between vibrations which play a large role in the experimental spectra.

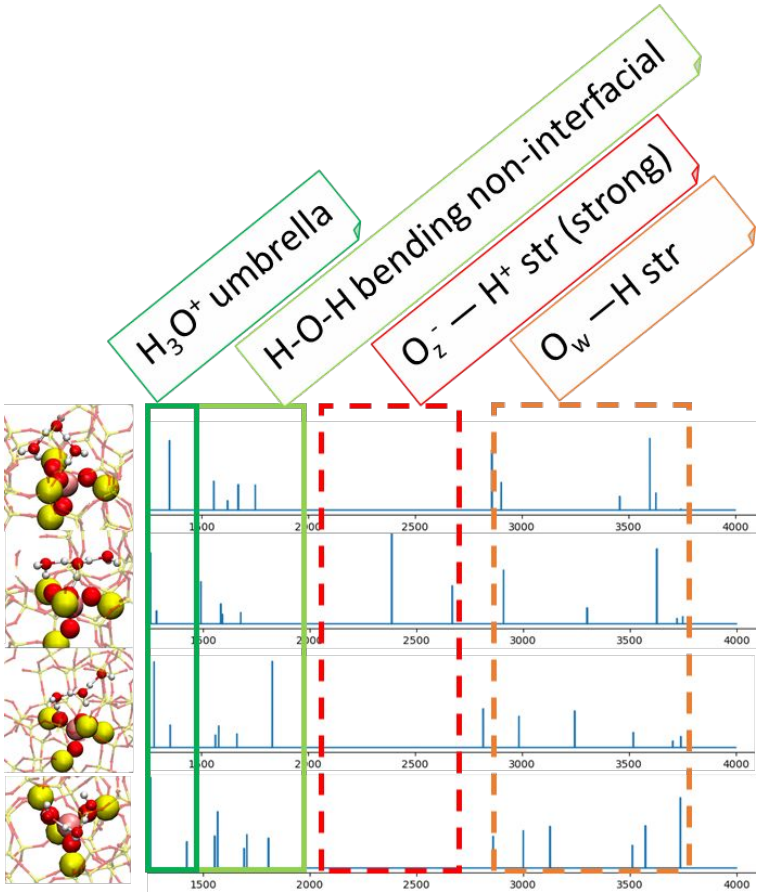

Figure S17. Same as S15 but for 3 H_2O cluster at the BAS. The ~1400 cm^{-1} mode (green) is instead a H_3O^+ umbrella mode.

S2e. Anharmonic spectral calculations

1 H_2O

For a 1 H_2O cluster, to relate the spectrum to the water cluster configuration, a representative structure with atom identities labeled is shown in Figure S18 with the H and O spectra. Only the "H 579" hydrogen atom spectrum spans over 1600 to 3000 cm^{-1}, and it agrees with the CEC spectrum, which indicates that the interfacial H contains the proton feature exclusively. The H and O spectra in the water moiety only shows a bending mode at ~1600 cm^{-1} and two free OH stretch modes at ~ 3700 cm^{-1}.

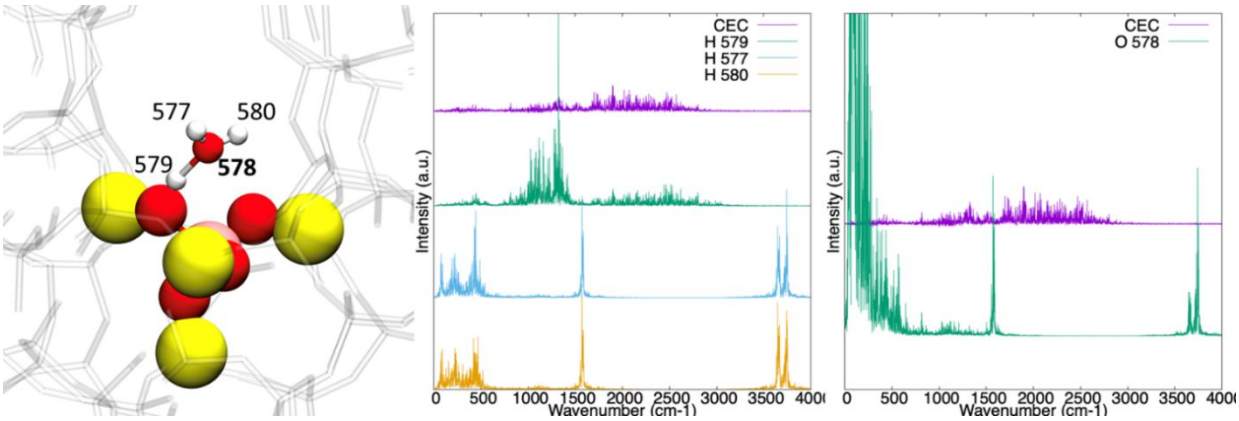

Figure S18. A representative configuration of 1 H_2O water cluster at the BAS (left), the hydrogen atom spectra (middle), and the oxygen atom spectra (right) compared to the CEC spectrum. The Si, O, Al, H atoms are colored in yellow, red, pink and white, respectively. The first 576 atoms form the zeolite framework and are not labeled for simplification. The H and O atom identities are labeled in normal and bold, respectively.

2 H_2O

For a 2 H_2O cluster, only the first configuration in Figure S16 has a large population, while the second and the third configurations only exist transiently. The vibrational spectrum of CEC is shown in the "H 579", "H 582", and "O 578" spectra, which are the interfacial H, the hydrogen bond H between two water molecules, and the interfacial O, respectively. For "H 577" and "O 581", there is no spectral density in the range of 2000~3000 cm^{-1}. Thus, the protonic charge is delocalized along the O_z--H_z-O_{w1}-H---(O_{w2}) axis.

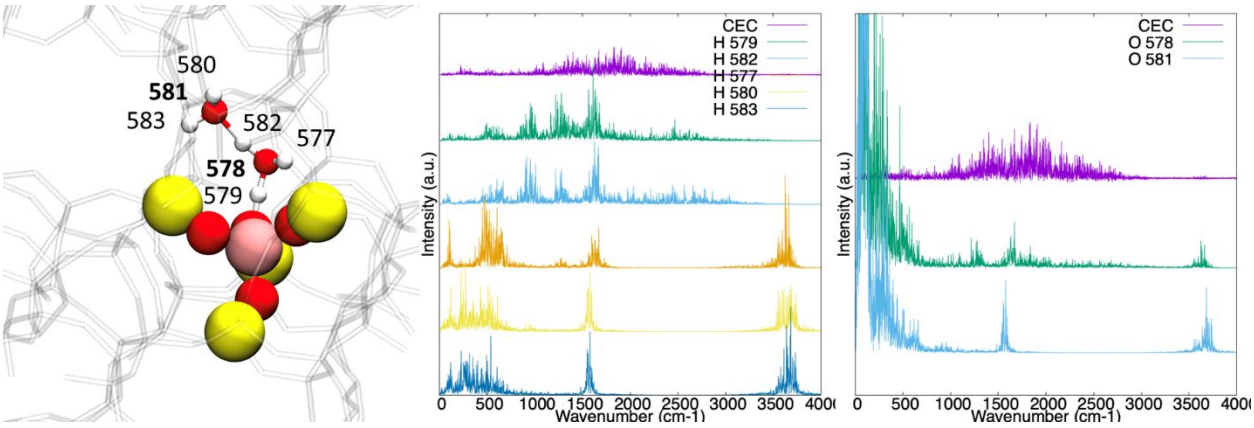

Figure S19. Same as Figure S18 but for 2 H_2O cluster at the BAS.

3 H_2O

For a 3 H_2O cluster, only the second and third configuration in Figure S17 have a large population; the first configuration is transient, and the fourth configuration has very low population. The spectral signature of the protonic charge is prominently expressed in the spectra of "O 584", "H 585", and "H 586", which are the O in the central water molecule and the two water-water hydrogen bond H, respectively. The interfacial H spectra, i.e., "H 577" and "H 580" also capture some of the proton spectrum features, but they mostly span between 3000 and 3700 cm^{-1}, which indicates that they behave as either hydrogen bond H or free OH during the trajectory.

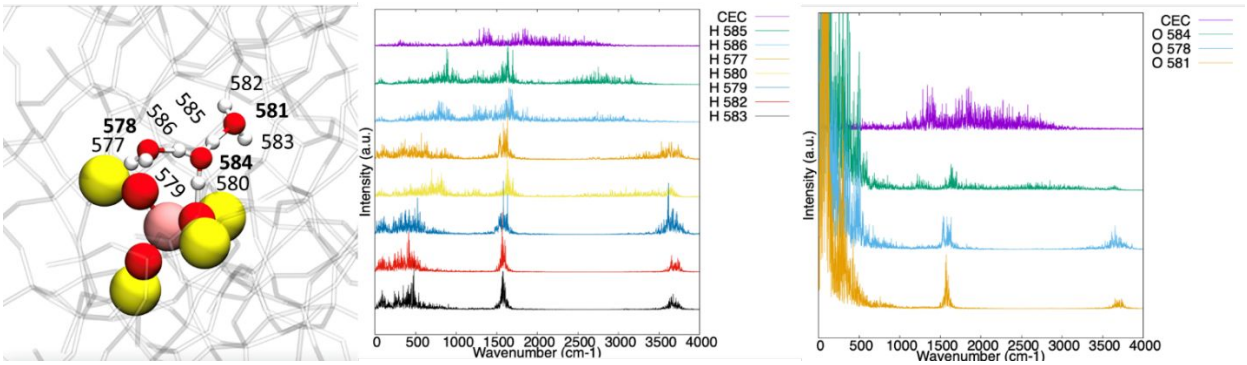

Figure S20. Same as Figure S18 but for 3 H_2O cluster at the BAS.

4 H_2O

For a 4 H_2O cluster, "O 584", "H 586", and "O 587" spectra exclusively show the protonic charge spectral signatures, which indicates that a protonic charge is still near the interface but mostly flanked by two water molecules, i.e. the protonic charge is delocalized along the $[O_{w1}\text{-}H\text{-}O_{w2}]^+$ axis.

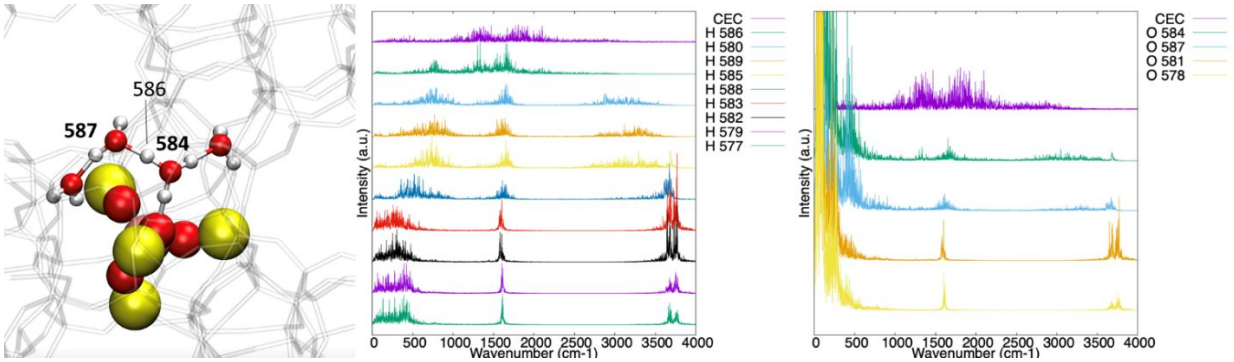

Figure S21. Same as Figure S18 but for 4 H_2O cluster at the BAS, and only the atoms showing protonic charge signatures are labeled.

6 H_2O

For a 6 H_2O cluster, the protonic charge vibrational signature is mostly shown in "O 581", "H 589", and "H 583", and somewhat in "O 587". We therefore assign this to an interchange of delocalized protonic charge between the $[H_{589}\text{-}O_{581}\text{-}H_{583}]$ and $[O_{587}\text{-}H_{589}\text{-}O_{581}]$ axes.

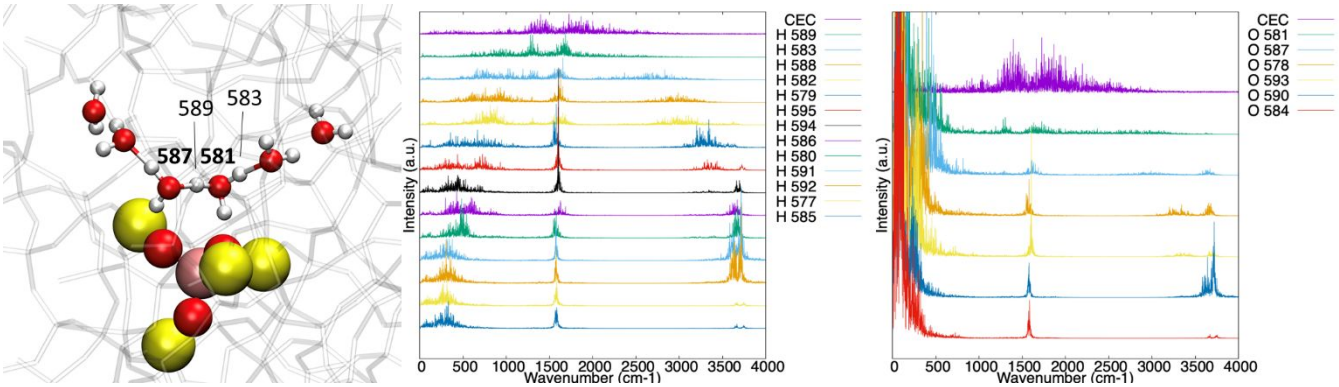

Figure S22. Same as Figure S21 but for 6 H_2O cluster at the BAS.

8 H_2O

For a 8 H_2O cluster, only “O 599”, “H 586”, “H 577”, and “H 601” shows the protonic charge vibrational signatures. The CEC is therefore no longer at the BAS interface, and instead resides near a water molecule which is triply-coordinated to three other water molecules.

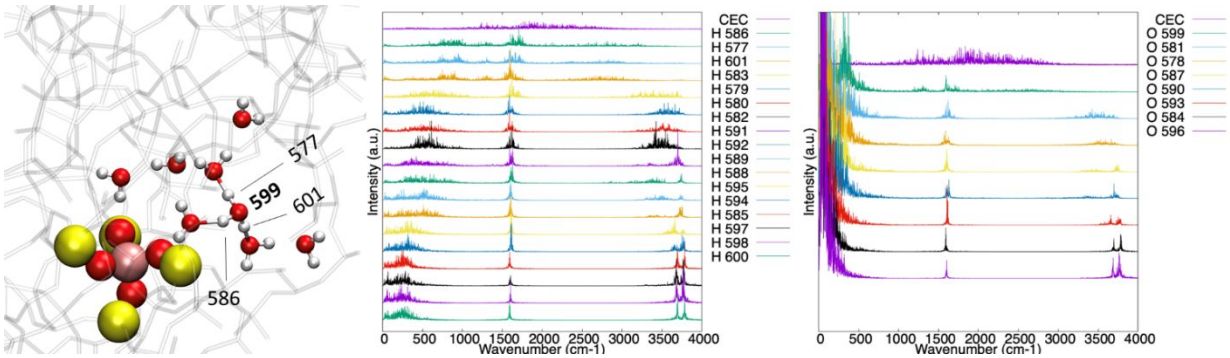

Figure S23. Same as Figure S21 but for 8 H_2O cluster at the BAS.

The fraction of H atoms contributing to the spectral density in the range of 2200~3200 cm^{-1} is larger at low hydration levels. The number of anharmonic H spectra that has spectral density covering this region is 1, 2, and 2 for the 1-3 H_2O clusters at the BAS, respectively. Divided by the total number of H spectra in each of these clusters, the population is 33.3%, 40.0%, and 28.6%, respectively. In the 6 and 8 H_2O cluster spectra, only 15.4% and 17.6% of all anharmonic H spectra span this frequency range.

CEC

In addition, comparison of the CEC spectra at various hydration levels is shown in Figure S24. For 1 H_2O, this result does not agree with the experiment as it does not reproduce the characteristic doublet near 2500 cm^{-1} and 2850 cm^{-1}. This is most likely a limitation of DFT for capturing the highly anharmonic nature of the underlying potential energy surface leading to the doublet feature. However, in the range of 2-8 H_2O the calculated CEC spectra with broad absorption spanning <3000 cm^{-1} are in much better agreement with both experimental spectra of hydrated zeolite and with previous studies on the excess proton in the liquid water.[9,13] Any changes in the CEC spectra with hydration are small compared to the linewidth of the feature and the noise level.

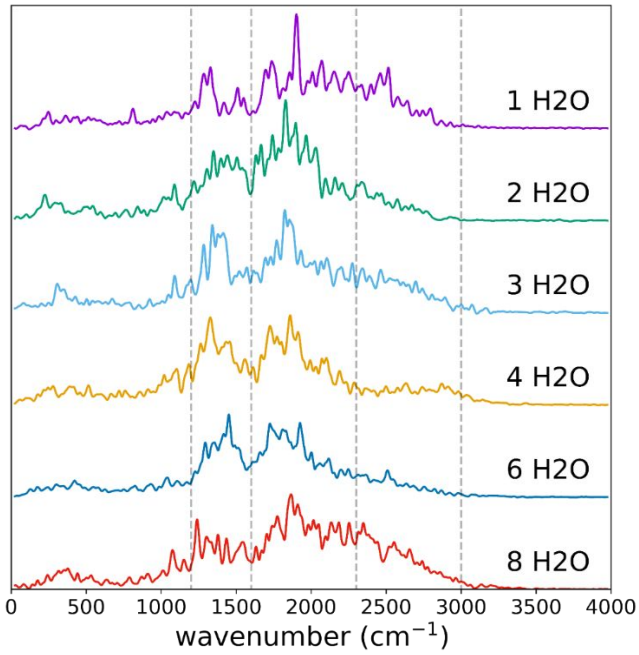

Figure S24. Comparison of the anharmonic CEC spectra calculated at 1-8 hydration levels in this work. A Hanning window with a window size of 50 cm^{-1} is convolved with the raw CEC spectra (calculated from eqn. S(26)) to yield smooth spectra. The vertical dashed line positions are 1200, 1600, 2300, and 3000 cm^{-1}.

S2f. Löwdin charge distributions

Figure S25 displays the Löwdin charge distributions calculated for clusters of 1-6 H_2O molecules. The connection between charge and local environment was assigned using the criteria in Table S2. Based on the configuration and protonic charge assignment, we can also understand the protonic charge position and delocalization based on the DFT charges distributions. In particular:

a. The Löwdin charge distributions in Fig. S25b-e confirm that the protonic charge rarely resides at the zeolitic O at hydration levels more than 2 H_2O molecules.
b. In the 2 H_2O cluster (Fig. S25b), the zeolitic O charge distribution shifted back towards the other Oz values with a long tail to the right indicating some charge sharing. One Ow is also
c. The Löwdin charge distributions of the 4 H_2O cluster (Fig. S25d) show that two water O and one H have significant proton charge signatures, which confirms a dominant configuration of shared proton between two O atoms, i.e., $[O_{w1}\text{-H-}O_{w2}]^+$.
d. Compared to Fig. S25d, the distribution of the 6 H_2O cluster (Fig. S25e) also shows that 3 O atoms have positive shifts in the Löwdin charges, i.e., the protonic charge is delocalized over three water molecules.

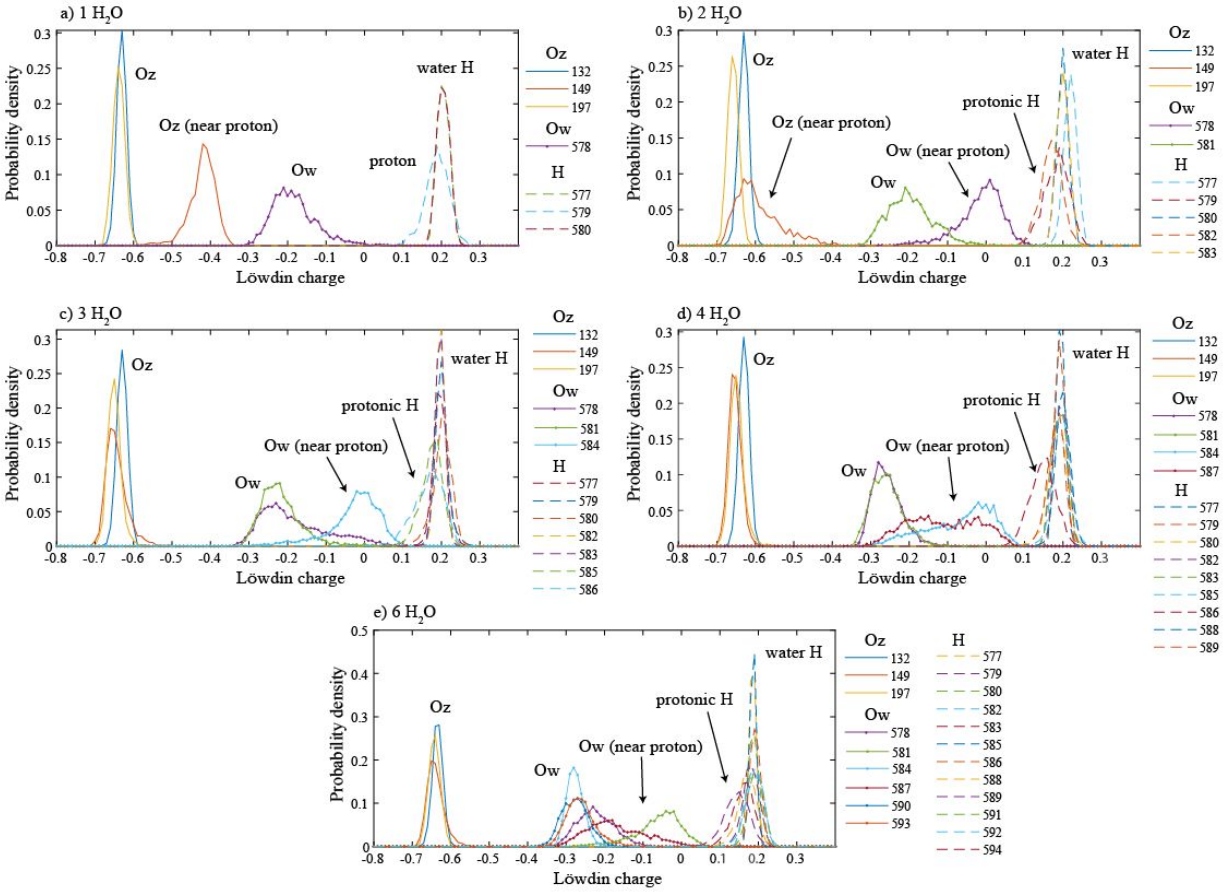

Figure S25. The normalized Löwdin charge distribution of zeolitic O, interfacial H, and the water O and H in clusters of a) 1 H_2O cluster at the BAS, b) 2 H_2O, c) 3 H_2O, d) 4 H_2O, and e) 6 H_2O.

Table S2. Assignment of the Löwdin charges to the O and H in the protonic water cluster and the BAS

Löwdin Charge	Assignment	Shape
-0.7 ~ -0.6	Zeolitic O (not adjacent to a protonic charge)	Narrow peak
-0.7 ~ -0.4	Zeolitic O (overlaps with a protonic charge)	Wide peak
-0.5 ~ -0.3	Zeolitic O (overlaps with a protonic charge)	Wide peak
-0.3 ~ 0.0	Water O (not adjacent to a protonic charge)	Wide peak
-0.2 ~ 0.1	Water O (overlaps with a protonic charge)	Wide peak
0.0 ~ 0.25	H (overlaps with a protonic charge)	Wide peak
0.15 ~ 0.25	H (not adjacent to a protonic charge)	Narrow peak

III. References

(1) Hack, J. H.; Dombrowski, J. P.; Ma, X.; Chen, Y.; Lewis, N. H. C.; Carpenter, W. B.; Li, C.; Voth, G. A.; Kung, H. H.; Tokmakoff, A. Structural Characterization of Protonated Water Clusters Confined in HZSM-5 Zeolites. *J. Am. Chem. Soc.* **2021**, *143* (27), 10203–10213. https://doi.org/10.1021/jacs.1c03205.

(2) Ison, A.; Gorte, R. J. The Adsorption of Methanol and Water on H-ZSM-5. *J. Catal.* **1984**, *89* (1), 150–158. https://doi.org/10.1016/0021-9517(84)90289-6.

(3) Widjaja, E.; Garland, M. Pure Component Spectral Reconstruction from Mixture Data Using SVD, Global Entropy Minimization, and Simulated Annealing. Numerical Investigations of Admissible Objective Functions Using a Synthetic 7-Species Data Set. *J. Comput. Chem.* **2002**, *23*, 911–919. https://doi.org/10.1002/jcc.10080.

(4) Eckstein, S.; Hintermeier, P. H.; Zhao, R.; Baráth, E.; Shi, H.; Liu, Y.; Lercher, J. A. Influence of Hydronium Ions in Zeolites on Sorption. *Angew. Chemie - Int. Ed.* **2019**, *58* (11), 3450–3455. https://doi.org/10.1002/anie.201812184.

(5) Carpenter, W. B.; Fournier, J. A.; Biswas, R.; Voth, G. A.; Tokmakoff, A. Delocalization and Stretch-Bend Mixing of the HOH Bend in Liquid Water. *J. Chem. Phys.* **2017**, *147* (8). https://doi.org/10.1063/1.4987153.

(6) Carpenter, W. B.; Fournier, J. A.; Lewis, N. H. C.; Tokmakoff, A. Picosecond Proton Transfer Kinetics in Water Revealed with Ultrafast IR Spectroscopy. *J. Phys. Chem. B* **2018**, *122* (10), 2792–2802. https://doi.org/10.1021/acs.jpcb.8b00118.

(7) De Marco, L.; Fournier, J. A.; Thämer, M.; Carpenter, W.; Tokmakoff, A. Anharmonic Exciton Dynamics and Energy Dissipation in Liquid Water from Two-Dimensional Infrared Spectroscopy. *J. Chem. Phys.* **2016**, *145* (9), 094501. https://doi.org/10.1063/1.4961752.

(8) Petersen, P. B.; Tokmakoff, A. Source for Ultrafast Continuum Infrared and Terahertz Radiation. *Opt. Lett.* **2010**, *35* (12), 1962. https://doi.org/10.1364/OL.35.001962.

(9) Li, C.; Swanson, J. M. J. Understanding and Tracking the Excess Proton in Ab Initio Simulations; Insights from IR Spectra. *J. Phys. Chem. B* **2020**, *124*, 5696–5708. https://doi.org/10.1021/acs.jpcb.0c03615.

(10) Li, C.; Voth, G. A. Using Constrained Density Functional Theory to Track Proton Transfers and to Sample Their Associated Free Energy Surface. *J. Chem. Theory Comput.* **2021**, *17*, 5759–5765. https://doi.org/10.1021/acs.jctc.1c00609.

(11) Endo, H.; Endo, Y. Spectral Analysis of the Velocity Autocorrelation Function of a Model Liquid. *Prog. Theor. Phys.* **1979**, *61* (6), 1569–1583. https://doi.org/10.1143/ptp.61.1569.

(12) Szabo, A.; Ostlund, N. S. *Modern Quantum Chemistry: Introduction to Advanced Electronic Structure Theory*; Courier Corporation, 2012.

(13) Biswas, R.; Carpenter, W.; Fournier, J. A.; Voth, G. A.; Tokmakoff, A. IR Spectral Assignments for the Hydrated Excess Proton in Liquid Water. *J. Chem. Phys.* **2017**, *146* (15). https://doi.org/10.1063/1.4980121.